ACS APPLIED MATERIALS & INTERFACES

Research Article

www.acsami.org

Rational Design of Magnetic Nanorattles as Contrast Agents for Ultrasound/Magnetic Resonance Dual-Modality Imaging

Peng Yang,[†] Fang Wang,[†] Xianfu Luo,[‡] Yuting Zhang,[†] Jia Guo,[†] Weibin Shi,[§] and Changchun Wang*[,†]

[†]State Key Laboratory of Molecular Engineering of Polymers, Department of Macromolecular Science, and Laboratory of Advanced Materials, Fudan University, Shanghai 200433, People's Republic of China

[‡]Department of Radiology, School of Medicine, Ruijin Hospital, Shanghai Jiaotong University, Shanghai 200025, People's Republic of China

[§]Xinhua Hospital Affiliated to Shanghai Jiaotong University School of Medicine, Shanghai 200092, People's Republic of China

ABSTRACT: Nanorattles, as promising functional hollow nanomaterials, show considerable advantages in a variety of applications for drug delivery, biosensors, and biomedical imaging because of their tailored ability in both the movable core and shell. In this study, we formulate a facile controllable route to synthesize a monodisperse magnetic nanorattle with an Fe_3O_4 superparticle as the core and poly(vinylsilane) (PVS) as the outer shell (Fe_3O_4@air@PVS) using the polymer-backbone-transition strategy. In the process of synthesis, besides acting as the precursor for the PVS shells of nanorattles, organosilica (o-SiO_2) plays the role of template for the middle cavities. The structures of nanorattles can be easily formed via etching treatment of NaOH solution. Through encapsulating sensitive perfluorohexane (PFH) in the cavities of Fe_3O_4@air@PVS, the biocompatible magnetic nanosystem shows a relatively stable ultrasound signal intensity and a high r_2 value of 62.19 mM^{-1} s^{-1} for magnetic resonance imaging (MRI). After intravenous administration of nanorattles to a healthy rat, dramatically positively enhanced ultrasound imaging and negatively enhanced T_2-weighted MRI are detected in the liver. Furthermore, when the Fe_3O_4@PFH@PVS nanorattles are administered to tumor-bearing mice, a significant passive accumulation in the tumor via an electron paramagnetic resonance effect is detected by both ultrasound imaging and MRI. In vivo experiments indicate that the obtained Fe_3O_4@PFH@PVS nanorattles can be used as dual-modality contrast agents for simultaneous ultrasound and MRI detection.

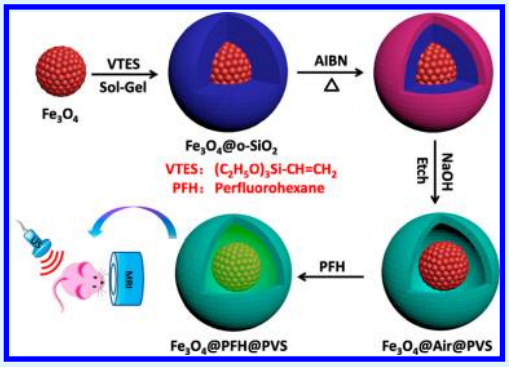

KEYWORDS: *nanorattle, iron oxide, contrast agent, ultrasound imaging, MRI*

1. INTRODUCTION

In the past few decades, the biomedical imaging technique has received much attention because of its powerful ability for analysis and diagnosis of targeting tissues.[1,2] To date, many bioimaging techniques, including ultrasound,[3] computed tomography (CT),[4] magnetic resonance imaging (MRI),[5] optical imaging,[6] single-photon emission computed tomography (SPECT),[7] and positron emission tomography (PET),[8] have been widely used in clinical diagnosis. These noninvasive imaging diagnosis tools not only achieve real-time visualization for living tissues but also can confirm early diseases such as cancers, heart disease, diabetes, and so on. However, each imaging technique has its intrinsic limitations, such as low spatial resolution or sensitivity, which is hardly overcome only by improving the imaging instrumentation.[9,10] Dual-modality imaging systems can not only combine the strengths of two imaging modalities but also eliminate each other's weakness, offering new opportunities for imaging, diagnostic improvements, and more accurate therapeutic monitoring.[2,11,12] Ultrasound imaging is practically free of geometric distortion and provides a real-time image but with low resolution.[13−15] It can help us rapidly diagnose a diseased region such as cancer, but its spatial resolution is low and cannot support accurate information on disease. Conversely, MRI has no tissue-penetrating limit and offers excellent tissue contrast and high spatial resolution but with insufficient sensitivity.[16−18] Thus, the tumor can be rapidly checked out via ultrasound imaging, and then a more complete and more accurate description of the anatomy information can be obtained through MRI. Ultrasound and MRI are complementary, and their combination can help increase intraoperative control and assessment in image-guided therapies.[19]

To obtain an information-rich image and improve the visibility of the image, a chemical compound known as a contrast agent or an imaging probe is usually introduced. Gas-filled microbubbles (MBs) stabilized by lipids, polymers, or silica, with a diameter of 1−8 μm, are usually used as ultrasound contrast agents (UCAs),[20,21] and superparamagnetic iron oxide (SPIO) nanoparticles, owing to their large magnetic moment, have been used for T_2-enhanced MRI.[22−25] Thus, SPIO

Received: April 27, 2014
Accepted: July 15, 2014
Published: July 15, 2014

nanoparticle-stabilized MBs as ultrasound/MRI dual-modality imaging contrast agents have attracted unprecedented attention for imaging investigations.[26−30] Nevertheless, the traditional MBs had undesirable aggregation in target tissues due to their overly large size and instability, which hindered the accurate response to the ultrasound imaging and MRI. Therefore, it is urgent and imperative to develop novel ultrasound/magnetic resonance dual-modality imaging contrast agents with nanoscale size for a better diagnosis effect and stronger ability to resist interference in tissues.

Rattle-type nanospheres (nanorattles), as promising functional hollow nanomaterials, have attracted more and more interest in drug delivery, biosensors, imaging, catalysis, and lithium ion batteries. Nanorattles have shown considerable advantages due to their tailored ability and functionality in both the core and shell.[31,32] Till now, many chemical and physicochemical methods have been developed to produce nanorattles. Usually, a core/shell nanoparticle including a core and two different shells is first synthesized, and then the middle layer is selectively removed through chemical dissolution or thermal calcination to form a rattle-type structure.[33−35] For success of the final desired structure, the fabrication often requires a large amount of work to carry out. Usually, the synthesis procedures are rather tedious, complex, and difficult for large-scale production.

Recently, our group developed a new polymer-backbone-transition method to fabricate uniform hollow composite microspheres with a controlled shell and size from vinyl-containing organosilica microspheres (VOMs).[36] By cross-linking the double bonds of VOMs with azobis-(isobutyronitrile) (AIBN) and then selective etching of the −Si−O− backbone with hydrofluoric acid (HF), the backbone network can be transformed from a −Si−O− chain to a −C−C− chain. The experimental results indicated that this kind of hollow polymer microsphere was very promising for ultrasound contrast agents. Meanwhile, our previous work reported two types of Fe_3O_4 superparticles that can be degraded in an acidic environment (pH 5.0).[37,38] These kinds of magnetic Fe_3O_4 superparticles may be ideal candidates for MRI contrast agents.

On the basis of our previous work, herein, we designed and synthesized a new type of monodisperse magnetic nanorattle with an Fe_3O_4 superparticle core and poly(vinylsilane) (PVS) shell (denoted Fe_3O_4@air@PVS nanorattle) using the polymer-backbone-transition approach. Various rattle-type structures with highly uniform particle sizes of about 400 nm and different shell thicknesses were successfully prepared. Compared with the general preparation methods of nanorattles, this approach did not require additional surface modification or activation steps, and was easy to scale up. Besides, this method can be extended as a general strategy to synthesize varying functional nanorattles. To obtain an excellent ultrasound signal, acoustic-sensitive perfluorohexane (PFH) was subsequently filled into the cavities as an ultrasound bubble generator. An in vitro cell experiment implied that the magnetic nanosystem had favorable biocompatibility. Furthermore, in vivo MR and ultrasound imaging studies clearly demonstrated that these magnetic nanorattles could successfully target the tumor and had great potential as novel dual-modality contrast agents for ultrasound and MRI to improve observation and diagnosis of cancer.

2. EXPERIMENTAL SECTION

2.1. Materials. Ammonium acetate (NH_4Ac), iron(III) chloride hexahydrate ($FeCl_3·6H_2O$), ethylene glycol (EG), anhydrous ethanol, sodium hydroxide, and aqueous ammonia solution (28%) were purchased from Shanghai Chemical Reagents Co. (China) and used as received. Vinyltriethoxysilane (VTES) was purchased from Sinopharm Chemical Reagent Co. Ltd. and used as received. Poly(γ-glutamic acid) (PGA) was purchased from Dingshunyin Biotechnology Co. (China) and used as received. AIBN was purchased from Sinopharm Chemical Reagent Co. Ltd. and recrystallized in ethanol. PFH was purchased from Acros Organics. Deionized water was used in all our experiments.

2.2. Preparation of Core−Shell Fe_3O_4@o-SiO_2 Nanoparticles. The PGA-modified Fe_3O_4 superparticles were synthesized through a solvothermal reaction as reported by our group.[37] Then PGA-modified Fe_3O_4 superparticles (100 mg) and VTES (0.5 mL) were added to H_2O (50 mL) under vigorous mechanical stirring (about 300 rpm) for 2 h. After that, a diluted ammonia solution (1.0 mL, water:ammonia = 4:1) was added to the above mixture dropwise using a microsyringe at a dripping speed of 1.5 mL h^{-1}. After the addition, the solution continued to react for 1 h at room temperature. The obtained Fe_3O_4@o-SiO_2 nanoparticles were then washed with deionized water and ethanol under ultrasonic conditions to remove the solvent and separated from the supernatant via a magnetic force during each washing step. The nanoparticles were dried in a vacuum dryer for 48 h and then stored at room temperature.

2.3. Preparation of Fe_3O_4@air@PVS Nanorattles. First, the core−shell Fe_3O_4@o-SiO_2 nanoparticles (100 mg) and AIBN (20 mg) were added to ethanol (50 mL), and the mixture was laid aside under a nitrogen atmosphere for 30 min and then heated to 80 °C under mechanical stirring (about 300 rpm) for 6 h. The shell-cross-linked Fe_3O_4@o-SiO_2 nanoparticles obtained were collected by using a magnetic force and dispersed in NaOH solution (0.5 wt %, 40 mL) for 3 h to etch the Si−O backbone to prepare Fe_3O_4@air@PVS nanorattles with a shell thickness of 25 nm. The nanorattles were washed several times with deionized water and ethanol under ultrasonic conditions to remove the solvent and separated from the supernatant via a magnetic force during each washing step. Finally, Fe_3O_4@air@PVS nanorattles were freeze-dried in a vacuum freeze-dryer for 48 h and then stored at room temperature.

2.4. Preparation of Fe_3O_4@PFH@PVS Nanorattles. A similar process of infusing PFH into nanorattles was followed by the method reported in ref 39. Typically, a bottle (5 mL) including Fe_3O_4@air@PVS nanorattles (20 mg) was added dropwise with the PFH liquid (50 μL). Then the mixture was sonicated in ice−water for 2 min to infuse the PFH into the cavities. Then Fe_3O_4@PFH@PVS was dispersed in a phosphate-buffered saline (PBS) solution (25 mL) under mechanical stirring (50 rpm) for 2 h. The Fe_3O_4@PFH@PVS nanorattles could be obtained via centrifugal separation and then dispersed in 10 mL of PBS for further use.

2.5. In Vitro Cell Viability Study. The in vitro cell viability of Fe_3O_4@PFH@PVS nanorattles was tested on HEK 293T cells via the MTT [3-(4,5-dimethylthiazol-2-yl)-2,5-diphenyltetrazolium bromide] method. Specifically, HEK 293T cells (100 μL) with a density of 1×10^4 cells per well were seeded in a 96-well flat culture plate and then incubated for 24 h. The Fe_3O_4@PFH@PVS nanorattles with different contents (0, 10, 50, 100, and 200 μg mL^{-1}) were added to the wells for 24 and 48 h. The MTT solution (5 μg mL^{-1} in PBS, 20 μL) was infused into the wells and then incubated for 4 h. The internalization of MTT was terminated through medium aspiration, and the HEK 293T cells were lysed using DMSO solution (150 μL). The absorbance of the mixture was measured using the ELISA (enzyme-linked immunosorbent assay) reader.

2.6. In Vitro Ultrasound Imaging and MRI. In vitro ultrasound images for PBS control and Fe_3O_4@PFH@PVS nanorattles under B mode were assessed using a color digital ultrasonic diagnostic apparatus (LOGIQ XP, GE, United States) with an 8L-RS probe (4−10 MHz, linear array). Typically, PBS solution (20 mL) with a constant concentration of samples (4 mg mL^{-1}) was filled into a

plastic bag (2.5 cm × 10.0 cm). The B mode imaging was tested under a frequency of 4 MHz, a pressure amplitude of 1.0 MPa, a pulse-repetition frequency (PRF) of 100 Hz, and an MI of 0.6 at 40% power.

The T_2-weighted MR image was acquired on a Siemens Magnetom Trio (3T, Siemens Medical Systems) with an eight-array loop coil. Fe_3O_4@PFH@PVS with different Fe concentrations (Fe concentration measured by ICP) in agarose solution was added to a series of tubes (2 mL) for T_2-weighted MR imaging under the following parameters: T_2-weighted spin−echo sequence, echo time (TE) of 19 ms, repetition time (TR) of 3000 ms, field of view (FOV) read of 180 mm, base resolution of 320, section thickness of 2.0 mm, and one acquisition. The relaxivity r_2 was calculated via fitting the curve of $1/T_2$ (s^{-1}) versus the Fe concentration (mM).

2.7. In Vivo Ultrasound and MRI. Animal experiments were performed according to the guidelines of the Regional Ethics Committee for Animal Procedures. The healthy rat and the pancreatic-tumor-bearing nude mouse (around 200−300 g of body mass) were obtained from the Shanghai Laboratory Animal Research Center and were fasted for 24 h before the experiments. The mice were first anesthetized using chloral hydrate (10%) and then fixed at the imaging system. Then the Fe_3O_4@PFH@PVS (0.5 mg/mL, 2 mL) PBS solution was injected via the tail vein. The scanning parameter setting was the same as for the in vitro ultrasound and MRI experiments. The livers and tumor regions of the nude mice were scanned before and after the injection of the Fe_3O_4@PFH@PVS nanorattles.

2.8. Characterization. Scanning electron microscopy (SEM) images were obtained using a TS-5136MM (TESCAN, Czech Republic) scanning electron microscope at an accelerating voltage of 20 kV. Transmission electron microscopy (TEM) images were obtained using an H-600 (Hitachi, Japan) transmission electron microscope at an accelerating voltage of 75 kV. Magnetic characterization was carried out on a model 6000 physical property measurement system (Quantum Design, Unites States) at 300 K. FTIR spectra were recorded on a Magna-550 (Nicolet, United States) spectrometer. Inductively coupled plasma (ICP) atomic emission spectra were recorded using a P-4010 (Hitachi, Japan) spectrometer.

3. RESULTS AND DISCUSSION

3.1. Synthesis and Characterization of Fe_3O_4@PFH@PVS Nanorattles. The whole procedure for the preparation of Fe_3O_4@air@PVS nanorattles is illustrated in Scheme 1. First, poly(γ-glutamic acid)-stabilized Fe_3O_4 superparticles prepared via the solvothermal method are evently coated with a new layer of organosilica (o-SiO_2) by a sol−gel reaction to prepare core−shell Fe_3O_4@o-SiO_2 nanoparticles. After that, the double bonds in the organosilica layers can be controllably cross-linked from the outermost layer to the inner layer via free radical polymerization using AIBN as the initiator to form a new outer layer of nanoparticles. Finally, the core−shell Fe_3O_4@o-SiO_2 nanoparticles can be converted into Fe_3O_4@air@PVS nanorattles through selectively dissolving the un-cross-linked o-SiO_2 middle layer with a certain amount of NaOH solution, along with transforming the polymer network of the outer layer from inorganic silicon−oxygen chains to organic carbon−carbon chains. Because the C═C double bonds of organosilica are derived from the precursor VTES, there was no further surface modification step required in both the cross-linking and outer-layer-forming procedures. In the whole synthesis process, besides acting as the precursor for the PVS shells of nanorattles, o-SiO_2 played the role of template for the middle cavities. At the same time, the formation of an outer layer and the removal of the template could be achieved through only one etching treatment, which was simple and easy to scale up. To enhance the signal of ultrasound imaging, we filled magnetic polymer nanorattles with ultrasonic-responsive PFH in their cavities (denoted Fe_3O_4@PFH@PVS). When Fe_3O_4@PFH@PVS was injected into the vessel of the mouse, the ultrasound energy could convert PFH into small bubbles through acoustic droplet vaporization (ADV) to create a strong imaging signal and increase the permeability of the vessel.[39−41] Then the accumulation of Fe_3O_4@PFH@PVS in tumor tissue was visualized and quantified using ultrasound and MR imaging.

The representative TEM images of PGA-stabilized Fe_3O_4 superparticles, core−shell Fe_3O_4@o-SiO_2 nanoparticles, and Fe_3O_4@air@PVS nanorattles are shown in Figure 1. As we can see, the PGA-stabilized Fe_3O_4 superparticles were uniform in both shape and size and the diameter of the superparticles was about 150 nm (Figure 1a). Then a layer of organosilica was introduced using VTES as the precursor by a sol−gel reaction, and monodisperse core−shell Fe_3O_4@o-SiO_2 nanoparticles, with a diameter of 400 nm, were formed (Figure 1b). After the Fe_3O_4@o-SiO_2 nanoparticles were etched with NaOH, the Fe_3O_4@air@PVS nanorattles obtained showed an excellent rattle-type structure with a uniform shell thickness (ca. 15 nm). The diameter did not obviously change compared with that of Fe_3O_4@o-SiO_2 (Figure 1c). The SEM image in Figure 1f revealed that the Fe_3O_4@air@PVS nanorattles possessed a smooth surface and uniform morphology, in which a sphere

Scheme 1. Schematic Illustration of the Preparation of Fe_3O_4@PFH@PVS Nanorattles as Dual-Modality Imaging Contrast Agents Using the Polymer-Backbone-Transition Method

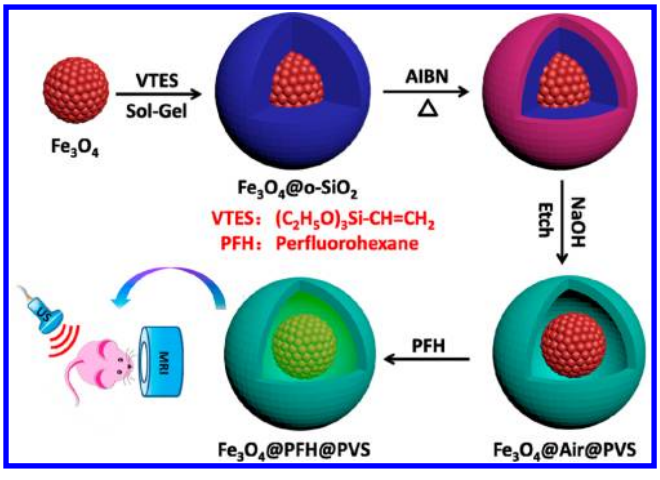

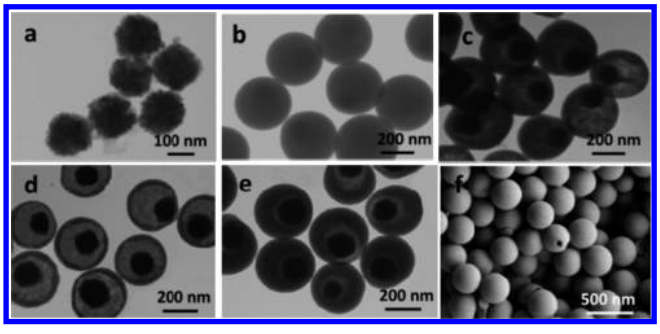

Figure 1. TEM images of (a) Fe_3O_4 superparticles, (b) core−shell Fe_3O_4@o-SiO_2 nanoparticles, and (c−e) Fe_3O_4@air@PVS nanorattles with different shell thicknesses of (c) 15 nm, (d) 25 nm, and (e) 80 nm. (f) SEM images of Fe_3O_4@air@PVS nanorattles with a shell thickness of 25 nm.

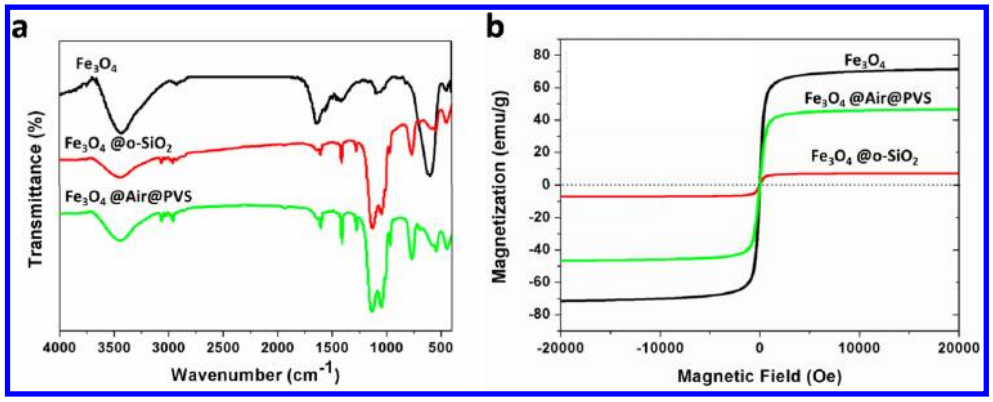

Figure 2. (a) FTIR spectra and (b) magnetization curves of PGA-stabilized Fe_3O_4 superparticles, Fe_3O_4@o-SiO_2 nanoparticles, and Fe_3O_4@air@PVS-25 nanorattles.

was broken, providing evidence of the hollow structure. Meanwhile, we have demonstrated in our previous study, in great detail, that the PVS shell thickness could be easily controlled via the relative ratio of the initiator to nanoparticles.[36] The higher the amount of the initiator, the thicker the shell. Here, we could control exactly the shell thickness of Fe_3O_4@air@PVS nanorattles by varying the amounts of AIBN in the cross-linking process. Maintaining a constant concentration of Fe_3O_4@o-SiO_2 nanoparticles, as the concentrations of AIBN increased from 0.2 to 0.4 and 2.0 mg/mL, the shell thicknesses of the Fe_3O_4@air@PVS nanorattles increased from 15 to about 25 and 80 nm, respectively (Figure 1c–e). To optimize the signal of MRI and PFH loading capability as well as prevent disruption of polymer shells under ultrasound pulses, we chose Fe_3O_4@air@PVS nanorattles with a modest shell thickness of 25 nm (denoted Fe_3O_4@air@PVS-25) as the research object.

The chemical components of Fe_3O_4@air@PVS nanorattles were identified with FTIR spectroscopy (Figure 2a). The peaks at 1630 and 1421 cm^{-1} from carboxylate groups indicated the presence of PGA on the surfaces of the Fe_3O_4 superparticles. The typical peaks at 438 and 573 cm^{-1} (Fe–O stretch) and a broad band at 3430 cm^{-1} (the O–H vibration) confirmed the existence of Fe_3O_4. Besides the characteristic peaks of Fe_3O_4 superparticles, bands appearing at 1149 and 1050 cm^{-1} corresponding to the Si–O stretch and peaks at 1602 and 767 cm^{-1} attributed to the C=C stretch and Si–C stretch were all found in the Fe_3O_4@air@PVS-25 nanorattles, corresponding to the existence of poly(vinylsilane). The magnetic characterization of Fe_3O_4 superparticles, core–shell Fe_3O_4@o-SiO_2 nanoparticles, and Fe_3O_4@air@PVS-25 nanorattles was conducted by vibrating sample magnetometry (VSM) at 300 K, and the values of saturation magnetization were 71.2, 7.1, and 46.5 emu/g, respectively (Figure 2b). The very small hysteresis loops confirmed the superparamagnetism of the Fe_3O_4@air@PVS-25 nanorattles, which indicated the potential of them as an MRI contrast agent.

To enhance the signal of ultrasound imaging, we filled the Fe_3O_4@air@PVS-25 nanorattles with PFH in their cavities (denoted Fe_3O_4@PFH@PVS). The PFH could generate highly echogenic phase-transitioned bubbles under ultrasound wave irritation.[39] Figure 3 shows digital photos of Fe_3O_4@PFH@PVS and free PFH with the same PFH concentration in PBS. An apparent phase-separated phenomenon could be observed in the free PFH–PBS solution due to the hydrophobicity of PFH (Figure 3a). Shaking PFH emulsions and allowing them

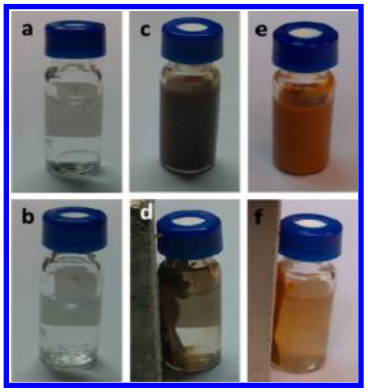

Figure 3. Digital photos of (a, b) PFH in PBS buffer solution, (c, d) Fe_3O_4 superparticles–PFH in PBS solution, and (e, f) Fe_3O_4@PFH@PVS in PBS solution. (d) and (f) were under a magnetic field.

to stand for a few minutes, we found that the PFH bubbles sunk to the bottle bottom (Figure 3b). In contrast, the Fe_3O_4@PFH@PVS solution was stable and homogeneous without PFH precipitation (Figure 3e). With attraction by a magnetic field, the Fe_3O_4@PFH@PVS solution became transparent and the nanorattles were gathered near the side of the magnet within 30 s, and no PFH subnatant remained in the solution (Figure 3f) compared with the Fe_3O_4 superparticle–PFH solution, in which PFH precipitation could be observed after magnetic attraction (Figure 3d). These results clearly demonstrated that the PFH was successfully infused into the cavities of Fe_3O_4@air@PVS-25 carriers and the Fe_3O_4@PFH@PVS possessed excellent dispersion stability and magnetic properties.

3.2. In Vitro Cell Viability Study. To guarantee the safety of Fe_3O_4@PFH@PVS used as an imaging contrast agent, an in vitro cell experiment on the normal HEK 293 cell line was carried out for a preliminary cytotoxicity assessment of Fe_3O_4@PFH@PVS (Figure 4). The viability of cells without nanorattles as the control was presumed to be 100%. There is no clear cell cytotoxicity in different concentrations of Fe_3O_4@PFH@PVS after 24 h of incubation. When the time was extended to 48 h, the viability of HEK 293T cells still remained 85% even at the highest concentration (200 mg mL^{-1}), implying that Fe_3O_4@PFH@PVS had favorable biocompatibility and the potential to be used as a medical agent.

3.3. In Vitro Ultrasound and MR Imaging. For investigating the contrast-intensified ultrasound imaging of Fe_3O_4@PFH@PVS, the PBS control and Fe_3O_4@PFH@PVS in PBS were wrapped up in plastic bags for the following

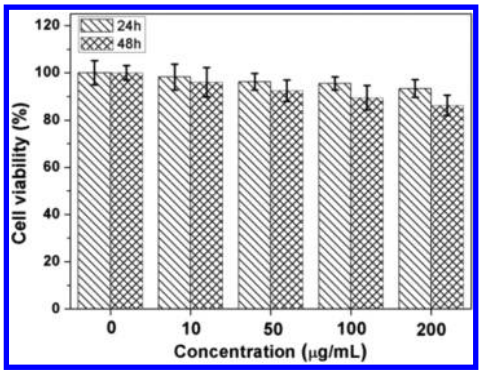

Figure 4. In vitro cell viability of HEK 293T cells incubated with Fe_3O_4@PFH@PVS at different concentrations for 24 and 48 h.

ultrasound imaging in vitro under the traditional B mode (Figure 5a,b). As we can see, the introduction of Fe_3O_4@PFH@PVS showed great backscatter signal enhancement compared with the PBS control, which has no response to the ultrasonic stimulation. Such a significant enhancement in ultrasound signal using Fe_3O_4@PFH@PVS was attributed to the high encapsulation capacity of PFH. The ability of Fe_3O_4@PFH@PVS nanorattles to enhance MRI in vitro was further measured by a clinical 3T MRI human clinical scanner. Figure 5c show a T_2-weighted MR image of Fe_3O_4@PFH@PVS nanorattles with different iron concentrations (Fe measured by ICP). The nanorattles showed a good MRI signal which was iron concentration dependent, with increased darkness as the concentration increased. The pseudocolored T_2-weighted MR image also showed a clearer view of the concentration-dependent negative enhancement effect (Figure 5d). As the molar concentration of Fe increased from 0.1 to 2.0 mM, the color in the MR image changed from kelly green to blue, indicating a change of the MRI signal density from low to high. We also obtained MR images of longitudinal sections of the samples (Figure 5e). As we can see, each image had a homogeneous signal strength, suggesting the hydrophilic Fe_3O_4@PFH@PVS nanorattles could be dispersed uniformly and stably in the solution, along with a relatively stable signal intensity, which ensured the availability of nanorattles as MRI negative contrast agents. The same concentration gradient of the Fe_3O_4@PFH@PVS solution was investigated for r_2 and calculated from the slope of the curve of $1/T_2$ (R_2) versus the Fe molar concentration. As shown in Figure 4f, R_2 showed an excellent linear relationship with the Fe concentration of Fe_3O_4@PFH@PVS. Finally, we obtained an r_2 value of 62.19 mM^{-1} s^{-1} for the nanorattles on the basis of the slope of the line.

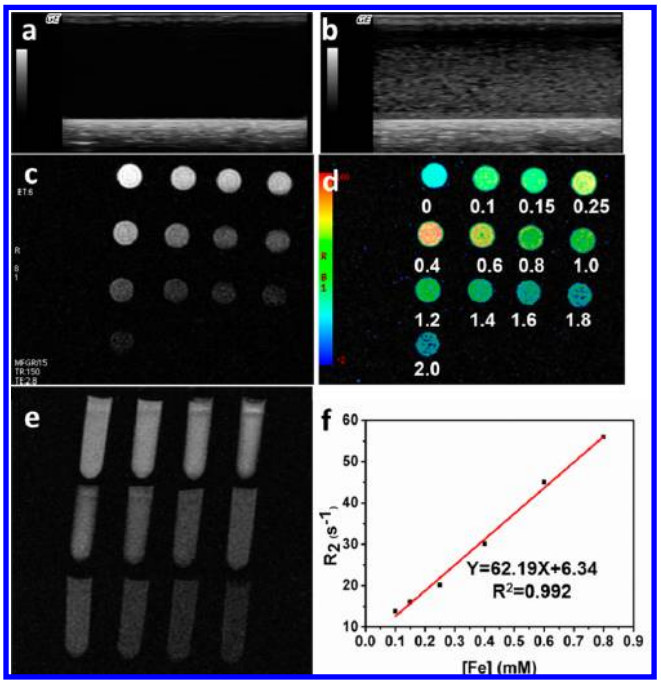

Figure 5. In vitro ultrasound imaging for (a) the PBS control and (b) Fe_3O_4@PFH@PVS nanorattles in PBS under B mode. (c) T_2-weighted, (d) pseudocolored mapped, and (e) longitudinal section in vitro MR images of Fe_3O_4@PFH@PVS with various molar concentrations of Fe. (f) Relaxation rate $1/T_2$ (R_2) versus different Fe molar concentrations (0.10, 0.15, 0.25, 0.40, 0.60, and 0.80 mM).

3.4. In Vivo Ultrasound and MRI. The dual-modality imaging ability of as-prepared Fe_3O_4@PFH@PVS nanorattles as the contrast agent for in vivo ultrasound and T_2-weighted MRI was evaluated using a healthy rat. As demonstrated in Figure 6, 5 min after injection of the nanorattles, we could clearly observe positively enhanced ultrasonic imaging (Figure 6b) and dramatically negatively enhanced T_2-weighted MR imaging (Figure 6d) in the liver tissue relative to those before injection (Figure 6a,c), which would be conducive to the detection of liver abnormalities, indicating the great potentials of the real-time property of the dual-bioimaging system.

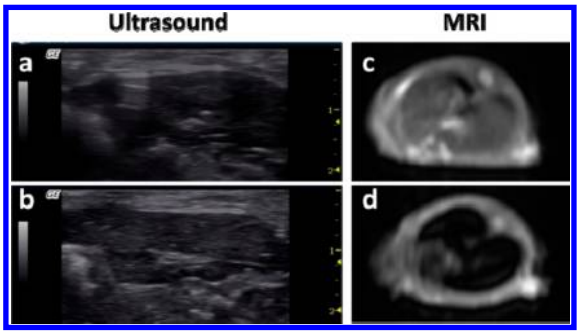

Figure 6. In vivo ultrasound scan and in vivo MRI of a healthy rat liver before (a, c) and after (b, d) injection of Fe_3O_4@PFH@PVS nanorattles.

To further assess in vivo tumor imaging of the nanorattles, ultrasound and T_2-weighted MRI were evaluated in pancreatic-tumor-bearing nude mouse before and after intravenous injection of Fe_3O_4@PFH@PVS (Figure 7). The ultrasound signal of tumor tissue was so low that the boundary of cancerous tissue and liver was very fuzzy before injection (Figure 7a). After caudal vein injection of Fe_3O_4@PFH@PVS, both liver and tumor tissues became brighter and the boundary on both sides became clearer (Figure 7b). Meanwhile, a significant darkening of the T_2-weighted MR image in the liver was clearly visible 5 min post intravenous injection (Figure 7d). One hour after the injection, Fe_3O_4 nanoparticles accumulated in the tumor via an EPR effect[42] and the tumor became darker as shown in Figure 7e. This indicted the magnetic nanorattles could penetrate through the blood vessels effectively and then enter tumor tissue due to poor lymphatic drainage and leaky vasculature in the tumor.[39]

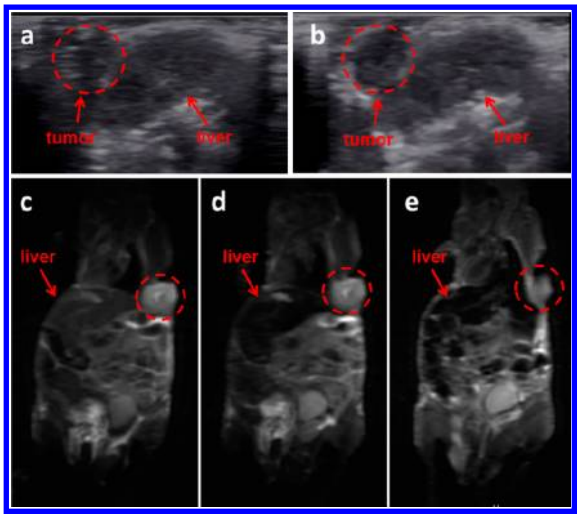

Figure 7. In vivo ultrasound scans of the tumor and liver of a nude mouse bearing a pancreatic tumor before (a) and after (b) injection of Fe_3O_4@PFH@PVS nanorattles under B mode. In vivo MR images of the same nude mouse before (c) and 5 min (c) and 1 h (e) after injection of contrast agents (red circled area for the tumor site).

4. CONCLUSION

In summary, we have reported a facile controllable route to synthesize magnetic PVS nanorattles using the polymer-backbone-transition strategy. The as-prepared nanorattles had a highly uniform particle size and an optimized shell thickness. In the whole synthesis, the organosilica not only played the role of precursor for the PVS shells of nanorattles, but also acted as the template for the middle cavities. The removal of the template and the formation of an outer layer were completed by a one-step etching treatment. Compared with the general preparation methods of nanorattles, this approach did not require additional surface modification or activation steps, which made it very simple and well suited for large-scale production. Besides, this strategy may be extended as a general method to synthesize varying functional nanorattles. Given the capability of magnetic nanoparticles for noninvasive T_2-weighed MRI, we used PGA-stabilized Fe_3O_4 superparticles as cores to fabricate magnetic nanorattles (Fe_3O_4@air@PVS), which could be used as a potential theranostic nanoplatform of simultaneous ultrasound and MR dual-modality imaging through successfully encapsulating PFH in the cavities. The cytotoxicity of Fe_3O_4@PFH@PVS on the normal HEK 293 cell line was examined, and the results revealed that this nanomaterial had no cytotoxicity with a concentration of up to 200 μg mL^{-1}. In vivo ultrasound and MRI experiments indicated the biocompatible Fe_3O_4@PFH@PVS nanorattles could rapidly reach the tumor tissue, thus effectively improving the diagnosis effect of cancers.

AUTHOR INFORMATION

Corresponding Author

*E-mail: ccwang@fudan.edu.cn.

Notes

The authors declare no competing financial interest.

ACKNOWLEDGMENTS

This work was supported by the National Science and Technology Key Project of China (Grant 2012AA020204), National Science Foundation of China (Grant 21034003), and Science and Technology Commission of Shanghai (Grants 13JC1400500 and 13520720200).

REFERENCES

(1) Sapsford, K. E.; Algar, W. R.; Berti, L.; Gemmill, K. B.; Casey, B. J.; Oh, E.; Stewart, M. H.; Medintz, I. L. Functionalizing Nanoparticles with Biological Molecules: Developing Chemistries That Facilitate Nanotechnology. *Chem. Rev.* **2013**, *113*, 1904−2074.

(2) Lee, D. E.; Koo, H.; Sun, I. C.; Ryu, J. H.; Kim, K.; Kwon, I. C. Multifunctional Nanoparticles for Multimodal Imaging and Theragnosis. *Chem. Soc. Rev.* **2012**, *41*, 2656−2672.

(3) Deshpande, N.; Needles, A.; Willmann, J. K. Molecular Ultrasound Imaging: Current Status and Future Directions. *Clin. Radiol.* **2010**, *65*, 567−581.

(4) Wang, L. V. Multiscale Photoacoustic Microscopy and Computed Tomography. *Nat. Photonics* **2009**, *3*, 503−509.

(5) Haacke, E. M.; Cheng, N. Y.; House, M. J.; Liu, Q.; Neelavalli, J.; Ogg, R. J.; Khan, A.; Ayaz, M.; Kirsch, W.; Obenaus, A. Imaging Iron Stores in the Brain Using Magnetic Resonance Imaging. *Magn. Reson. Imaging* **2005**, *23*, 1−25.

(6) Fang, N.; Lee, H.; Sun, C.; Zhang, X. Sub-Diffraction-Limited Optical Imaging with a Silver Superlens. *Science* **2005**, *308*, 534−537.

(7) Hooly, T. A.; Abbott, B. G.; Al-Mallah, M.; Calnon, D. A.; Cohen, M. C.; DiFilippo, F. P.; Ficaro, E. P.; Freeman, M. R.; Hendel, R. C.; Jain, D. Single Photon-Emission Computed Tomography. *J. Nucl. Cardiol.* **2010**, *17*, 941−973.

(8) Terasawa, T.; Lau, J.; Bardet, S.; Couturier, O.; Hotta, T.; Hutchings, M.; Nihashi, T.; Nagai, H. Fluorine-18-Fluorodeoxyglucose Positron Emission Tomography for Interim Response Assessment of Advanced-Stage Hodgkin's Lymphoma and Diffuse Large B-Cell Lymphoma: A Systematic Review. *J. Clin. Oncol.* **2009**, *27*, 1906−1914.

(9) Louie, A. Multimodality Imaging Probes: Design and Challenges. *Chem. Rev.* **2010**, *110*, 3146−3195.

(10) Brigger, I.; Dubernet, C.; Couvreur, P. Nanoparticles in Cancer Therapy and Diagnosis. *Adv. Drug Delivery Rev.* **2002**, *54*, 631−651.

(11) Wang, X.; Liu, H.; Chen, D.; Meng, X.; Liu, T.; Fu, C.; Hao, N.; Zhang, Y.; Wu, X.; Ren, J.; Tang, F. Q. Multifunctional Fe_3O_4@P(St/MAA)@Chitosan@Au Core/Shell Nanoparticles for Dual Imaging and Photothermal Therapy. *ACS Appl. Mater. Interfaces* **2013**, *5*, 4966−4971.

(12) Zhang, H. C.; Ma, X.; Nguyen, K. T.; Zhao, Y. L. Biocompatible Pillararene-Assembly-Based Carriers for Dual Bioimaging. *ACS Nano* **2013**, *7*, 7853−7863.

(13) Deshpande, N.; Needles, A.; Willmann, J. K. Molecular Ultrasound Imaging: Current Status and Future Directions. *Clin. Radiol.* **2010**, *65*, 567−581.

(14) Tang, M. X.; Mulvana, H.; Gauthier, T.; Lim, A. K.; Cosgrove, D. O.; Eckersley, R. J.; Stride, E. Quantitative Contrast-Enhanced Ultrasound Imaging: A Review of Sources of Variability. *Interface Focus* **2011**, *1*, 520−539.

(15) Mitragotri, S.; Kost, J. Low-Frequency Sonophoresis: A Review. *Adv. Drug Delivery Rev.* **2004**, *56*, 589−601.

(16) Bassera, P. J.; Pierpaoli, C. Microstructural and Physiological Features of Tissues Elucidated by Quantitative-Diffusion-Tensor MRI. *J. Magn. Reson.* **2011**, *213*, 560−570.

(17) Modo, M.; Hoehn, M.; Bulte, J. W. Cellular MR Imaging. *Mol. Imaging* **2005**, *4*, 143−164.

(18) Caravan, P. Strategies for Increasing the Sensitivity of Gadolinium Based MRI Contrast Agents. *Chem. Soc. Rev.* **2006**, *35*, 512−523.

(19) Feinberg, D. A.; Giese, D.; Bongers, D. A.; Ramanna, S.; Zaitsev, M.; Markl, M.; Günther, M. Hybrid Ultrasound MRI for Improved Cardiac Imaging and Real-Time Respiration Control. *Magn. Reson. Med.* **2010**, *63*, 290−296.

(20) Lin, P. L.; Eckersley, R. J.; Hall, E. A. Ultrabubble: A Laminated Ultrasound Contrast Agent with Narrow Size Range. *Adv. Mater.* **2009**, *21*, 3949−3952.

(21) Lindner, J. R. Microbubbles in Medical Imaging: Current Applications and Future Directions. *Nat. Rev. Drug Discovery* **2004**, *3*, 527−533.
(22) Lee, N.; Hyeon, T. Designed Synthesis of Uniformly Sized Iron Oxide Nanoparticles for Efficient Magnetic Resonance Imaging Contrast Agents. *Chem. Soc. Rev.* **2012**, *41*, 2575−2589.
(23) Na, H. B.; Song, I. C.; Hyeon, T. Inorganic Nanoparticles for MRI Contrast Agents. *Adv. Mater.* **2009**, *21*, 2133−2148.
(24) Guo, J.; Yang, W. L.; Wang, C. C. Magnetic Colloidal Supraparticles: Design, Fabrication and Biomedical Applications. *Adv. Mater.* **2013**, *25*, 5196−5214.
(25) Xuan, S.; Wang, F.; Lai, J.; Sham, K.; Wang, Y.; Lee, S.; Yu, J.; Cheng, C.; Leung, K. Synthesis of Biocompatible, Mesoporous Fe_3O_4 Nano/Microspheres with Large Surface Area for Magnetic Resonance Imaging and Therapeutic Applications. *ACS Appl. Mater. Interfaces* **2011**, *3*, 237−244.
(26) Yang, F.; Li, X. Y.; Chen, Z. P.; Zhang, Y.; Wu, J. R.; Gu, N. Superparamagnetic Iron Oxide Nanoparticle-Embedded Encapsulated Microbubbles as Dual Contrast Agents of Magnetic Resonance and Ultrasound Imaging. *Biomaterials* **2009**, *30*, 3882−3890.
(27) Chow, A. M.; Chan, K. W.; Cheung, J. S.; Wu, E. X. Enhancement of Gas-Filled Microbubble R2* by Iron Oxide Nanoparticles for MRI. *Magn. Reson. Med.* **2010**, *63*, 224−229.
(28) Liu, Z.; Lammers, T.; Ehling, J.; Fokong, S.; Bornemann, J.; Kiessling, F.; Gätjens, J. Iron Oxide Nanoparticle-Containing Microbubble Composites as Contrast Agents for MR and Ultrasound Dual-Modality Imaging. *Biomaterials* **2011**, *32*, 6155−6163.
(29) Sun, Y.; Zheng, Y.; Ran, H.; Zhou, Y.; Shen, H.; Chen, Y.; Chen, H.; Krupka, T. M.; Li, A.; Li, P.; Wang, Z. Superparamagnetic PLGA-Iron Oxide Microcapsules for Dual-Modality US/MR Imaging and High Intensity Focused US Breast Cancer Ablation. *Biomaterials* **2012**, *33*, 5854−5864.
(30) Huang, H. Y.; Hu, S. H.; Hung, S. Y.; Chiang, C. S.; Liu, H. L.; Chiou, T. L.; Chen, S. Y. SPIO Nanoparticle-Stabilized PAA-F127 Thermosensitive Nanobubbles with MR/US Dual-Modality Imaging and HIFU-Triggered Drug Release for Magnetically Guided in Vivo Tumor Therapy. *J. Controlled Release* **2013**, *172*, 118−127.
(31) Zhao, Y.; Jiang, L. Hollow Micro/Nanomaterials with Multilevel Interior Structures. *Adv. Mater.* **2009**, *21*, 3621−3689.
(32) Lou, X. W.; Archer, L. A.; Yang, Z. C. Hollow Micro-/Nanostructures: Synthesis and Applications. *Adv. Mater.* **2008**, *21*, 3987−4019.
(33) Zhou, W. D.; Yu, Y. C.; Chen, H.; DiSalvo, F. J.; Abruna, H. D. Yolk-Shell Structure of Polyaniline-Coated Sulfur for Lithium-Sulfur Batteries. *J. Am. Chem. Soc.* **2013**, *135*, 16736−16743.
(34) Chen, D.; Li, L. L.; Tang, F. Q.; Qi, S. Facile and Scalable Synthesis of Tailored Silica "Nanorattle" Structures. *Adv. Mater.* **2009**, *21*, 3804.
(35) Linley, S.; Leshuk, T.; Gu, F. X. Synthesis of Magnetic Rattle-Type Nanostructures for Use in Water Treatment. *ACS Appl. Mater. Interfaces* **2013**, *5*, 2540−2548.
(36) Yang, P.; Ding, J.; Guo, J.; Shi, W. B.; Hu, J.; Wang, C. C. A Strategy for Fabrication of Uniform Double-Shell Hollow Microspheres as Effective Acoustic Echo Imaging Contrast Agents through a New Polymer-Backbone-Transition Method. *J. Mater. Chem. B* **2013**, *1*, 544−551.
(37) Luo, B.; Xu, S.; Luo, A.; Wang, W. R.; Wang, S. L.; Guo, J.; Lin, Y.; Zhao, D. Y.; Wang, C. C. Mesoporous Biocompatible and Acid-Degradable Magnetic Colloidal Nanocrystal Clusters with Sustainable Stability and High Hydrophobic Drug Loading Capacity. *ACS Nano* **2011**, *5*, 1428−1435.
(38) Li, D.; Tang, J.; Wei, C.; Guo, J.; Wang, S. L.; Chaudhary, D.; Wang, C. C. Doxorubicin-Conjugated Mesoporous Magnetic Colloidal Nanocrystal Clusters Stabilized by Polysaccharide as a Smart Anticancer Drug Vehicle. *Small* **2012**, *8*, 2690−2697.
(39) Wang, X.; Chen, H. R.; Zheng, Y. Y.; Ma, M.; Chen, Y.; Zhang, K.; Zeng, D. P.; Shi, J. L. Au-Nanoparticle Coated Mesoporous Silica Nanocapsule-Based Multifunctional Platform for Ultrasound Mediated Imaging, Cytoclasis and Tumor Ablation. *Biomaterials* **2013**, *34*, 2057−2068.
(40) Wang, X.; Chen, H. R.; Chen, Y.; Ma, M.; Zhang, K.; Li, F. Q.; Zheng, Y. Y.; Zeng, D. P.; Wang, Q.; Shi, J. L. Perfluorohexane-Encapsulated Mesoporous Silica Nanocapsules as Enhancement Agents for Highly Efficient High Intensity Focused Ultrasound (HIFU). *Adv. Mater.* **2012**, *24*, 785−791.
(41) Yang, P.; Li, D.; Jin, S.; Ding, J.; Guo, J.; Shi, W. B.; Wang, C. C. Stimuli-Responsive Biodegradable Poly(methacrylic acid) Based Nanocapsules for Ultrasound Traced and Triggered Drug Delivery System. *Biomaterials* **2014**, *35*, 2079−2088.
(42) Zeng, X.; Sun, Y. X.; Zhang, X. Z.; Zhuo, R. X. Biotinylated Disulfide Containing PEI/Avidin Bioconjugate Shows Specific Enhanced Transfection Efficiency in Hepg2 Cells. *Org. Biomol. Chem.* **2009**, *7*, 4201−4210.